Complex networks for tracking extreme rainfall during typhoons

U. Ozturk, N. Marwan, O. Korup, H. Saito, A. Agarwal, M. J. Grossman, M. Zaiki, and J. Kurths

Citation: Chaos **28**, 075301 (2018); doi: 10.1063/1.5004480
View online: https://doi.org/10.1063/1.5004480
View Table of Contents: http://aip.scitation.org/toc/cha/28/7
Published by the American Institute of Physics

Complex networks for tracking extreme rainfall during typhoons

U. Ozturk,[1,2,a)] N. Marwan,[1] O. Korup,[2] H. Saito,[3] A. Agarwal,[1,2,4] M. J. Grossman,[5] M. Zaiki,[6] and J. Kurths[1,7]
[1]*Potsdam Institute for Climate Impact Research – PIK, Potsdam D-14476, Germany*
[2]*Institute of Earth and Environmental Science, University of Potsdam, Potsdam D-14473, Germany*
[3]*College of Economics, Kanto Gakuin University, Yokohama 236-8501, Japan*
[4]*Helmholtz Centre Potsdam, German Research Centre for Geosciences – GFZ, Potsdam D-14476, Germany*
[5]*Department of Geography, Southern Illinois University Edwardsville, Edwardsville, Illinois 62026, USA*
[6]*Department of Economics and Management, Seikei University, Tokyo 180-8633, Japan*
[7]*Department of Physics, Humboldt University, Berlin D-12489, Germany*

(Received 13 September 2017; accepted 28 November 2017; published online 6 July 2018)

Reconciling the paths of extreme rainfall with those of typhoons remains difficult despite advanced forecasting techniques. We use complex networks defined by a nonlinear synchronization measure termed event synchronization to track extreme rainfall over the Japanese islands. Directed networks objectively record patterns of heavy rain brought by frontal storms and typhoons but mask out contributions of local convective storms. We propose a radial rank method to show that paths of extreme rainfall in the typhoon season (August-November, ASON) follow the overall southwest-northeast motion of typhoons and mean rainfall gradient of Japan. The associated eye-of-the-typhoon tracks deviate notably and may thus distort estimates of heavy typhoon rainfall. We mainly found that the lower spread of rainfall tracks in ASON may enable better hindcasting than for westerly-fed frontal storms in June and July. *Published by AIP Publishing.* https://doi.org/10.1063/1.5004480

Complex network is a special type of graph describing meaningful interactions of real life systems (e.g., social, biological); it is also a popular tool to investigate the spatiotemporal dynamics of climate systems, such as extreme precipitation. Tropical storms incur substantial losses each year, particularly in the western Pacific. Despite many advances in their monitoring and forecasting, the dynamics of extreme rainfall patterns remains partly unresolved. We use complex networks for investigating how extreme rainfall correlates in space and time during the passage of tropical storm over the Japanese archipelago. We found that the rainfall tracks consistently diverge from eye-of-the-typhoon tracks, while the mean difference in track azimuths decreases from frontal storm (June-July) to typhoon seasons (August-November). This outcome might increase the predictability of the extreme precipitation during the typhoon season.

I. INTRODUCTION

The Northwest Pacific has the world's highest frequency of tropical storms, and Japan is hit by an average of 26 tropical storms (defined as having sustained wind speeds >17 m/s, and referred to here as "typhoon") each year according to the Japan Meteorological Agency (JMA). Together with extra-tropical lows, the Baiu Front and local convection cells bring nearly 75% of Japan's total annual precipitation between April and October.[1,2] Yet typhoons and the Baiu Front are largely responsible for the highest rainfalls.[3] The Baiu Front brings early summer rainfall as part of the Asian monsoonal system.[4] The front extends from eastern China east-northeastward into the Pacific following the island arc of Japan and forms where warm maritime tropical air mass intersects with cool polar maritime air.[5] Polar and subtropical jets push this moisture eastwards onto Japan from early June to late July.[6] This eastward moisture flow at around 35°N is unique in the northern hemisphere.[7] Except for Hokkaido, most of Japan experiences Baiu-derived heavy rainfall, which is most pronounced in Kyushu,[5] shown with the colors light green to red tones in Fig. 1(c). Typhoons also have links to the Asian monsoon and the Madden-Julian Oscillation[8,9] and bring heavy rainfall from August to November.

Recent studies suggest that typhoon tracks in the Northwest Pacific have shifted west towards South Korea since the 1950s with rising intensities.[10,11] The number of typhoons that make landfall in Japan grows according to the scenarios of the Intergovernmental Panel for Climate Change.[12,13] Hence, quantifying the tracks and intensities of extreme rainfall is essential for informing quantitative assessments of concomitant flood and landslide hazards. Previous work identified major eye-of-the-typhoon (center of the tropical storm) tracks (ETTs) over Japan[14,15] and interpreted their temporal trends as proxies for atmospheric warming.[16] Several approximately stationary long lasting downpour structures (rainbands) evolve around the eye-of-the-typhoon.[17,18] Rain structures around the eye wall up to 100 km are distributed nearly symmetrically,[19] and they behave asymmetrically in increasing distance from the eye.[20,21] The ETTs deviate from those of extreme rainfall and a proposed "docked inner rain shield" mainly within 150-250 km northeast to southeast of the eye, and a rarer "outer rain shield" up to 500 km northwest to southwest of the eye.[22] Yet this phenomenon awaits further systematic documentation and tracking.

a) Author to whom correspondence should be addressed: ugur.oeztuerk@uni-potsdam.de

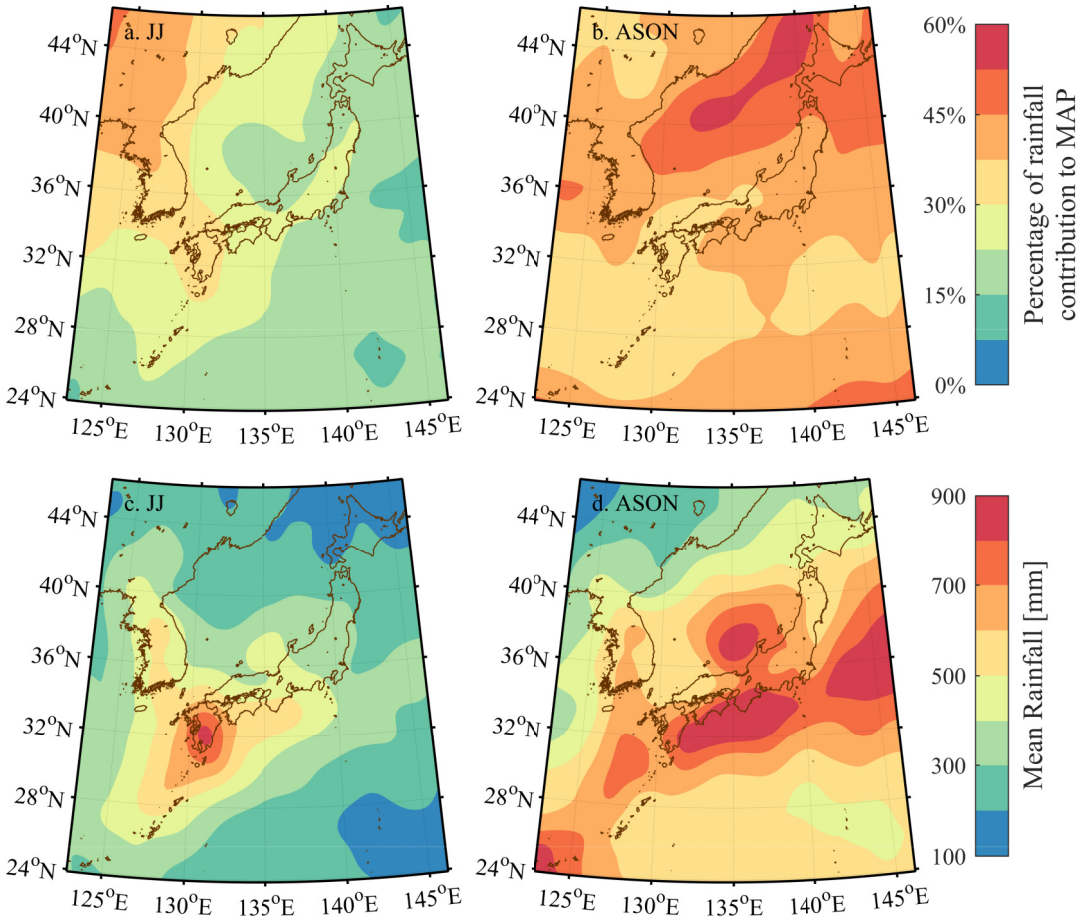

FIG. 1. Rainfall distribution in the study area based on the TRMM data. (a) and (b) Ratio of rainfall during JJ and ASON and mean annual rainfall (MAP, 1998-2015). (c) and (d) Mean annual rainfall in JJ and ASON.

To approach this problem of objectively capturing rainfall trajectories (information transfer) alongside the ETTs, we use complex networks, an approach that has recently emerged for analyzing geoscientific data,[23] particularly in climate science,[24,25] hydrology,[26–29] seismology,[30] and geomorphology.[31] Such networks capture the dynamics (information flow) of vertical wind field interactions,[32] decadal climate variability,[33] or extreme floods.[34]

Our aim is to use complex networks to objectively and consistently track extreme rainfall caused by tropical and frontal storms over Japan (causal links), and to check for systematic offsets from EETs. The underlying idea is to determine the correlation between rainfall time series at gridded geographic locations. Two locations are linked if their correlation coefficient exceeds a defined threshold.[35] Network analysis focuses mostly on the existence of such edges instead of the details of their interaction, though edges can be weighted by their correlation strength.[36,37] All edges form an adjacency matrix to encode a complex network.[38] Cumulative rainfall data are mostly heavy tailed,[39] calling for non-linear functions to capture correlations between event series.[40,41] Event synchronization (ES) is an intermediate non-linear tool to detect delayed correlation between spatially separated event series.[42] Complex networks based on ES express the correlation between extreme rainfall events such as those during the South Asian[43] or South American[34,44] monsoons and yield good agreement with modeled wind directions from National Centers for Environmental Prediction (NCEP) and National Center for Atmospheric Research (NCAR) or Modern Era Retrospective-analysis for Research and Applications (MERRA) reanalysis data.

II. DATA

We analyzed satellite-derived daily (1998-2015) rainfall estimates from the Tropical Rainfall Measuring Mission (TRMM 3B42V7) at 0.25° spatial resolution.[45] We split the data into those linked to the Baiu frontal storm season from June 1 to July 31 [JJ, Figs. 1(a) and 1(c)] and those linked to the typhoon season from August 1 to November 30 [ASON, Figs. 1(b) and 1(d)],[5] defining rainfalls above the 95th percentile as extreme.[46,47] The Regional Specialized Meteorological Center (RSMC) in Tokyo and the Japanese Meteorological Agency (JMA) provide ETT data (1998-2015), including storm names, dates, and geographic positions of the eye at 6-hourly intervals for sustained wind speeds >17 m/s (Fig. 2).

III. METHODS

Event synchronization (ES) and the radial ranks R_{ij}^{r} are used together to estimate the information flow on a network in order to track the extreme rainfall. ES is characterized by

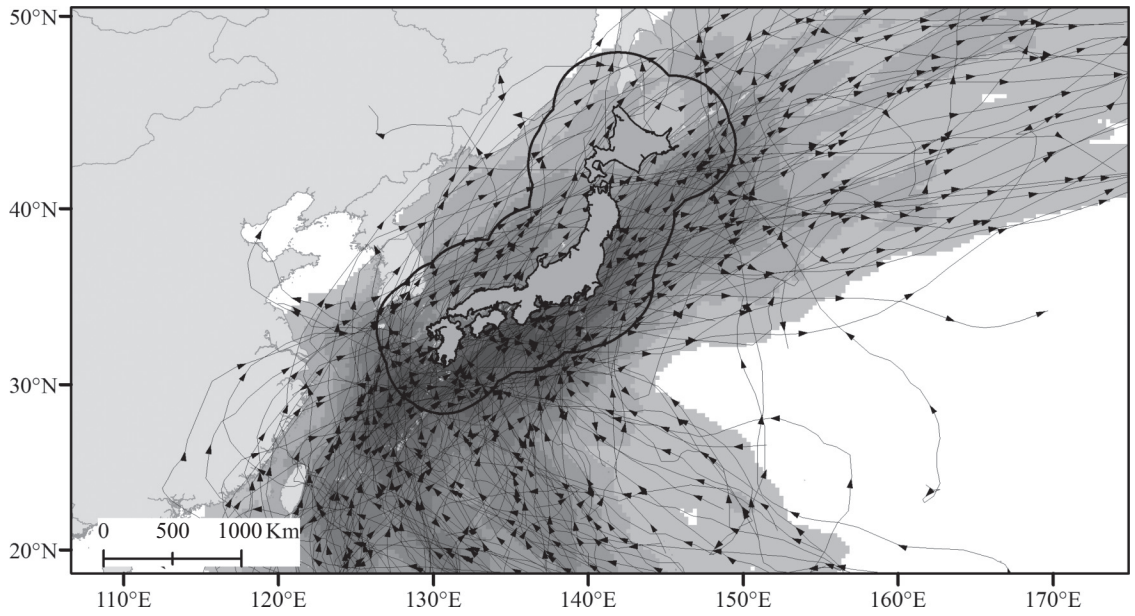

FIG. 2. Tracks of tropical storms that came within 300 km of the four main islands of Japan between 1998 and 2015. Darker shades indicate higher density of tracks.

a time-delay parameter q_{ij} and a strength parameter Q_{ij} (Sec. III A). We used q_{ij} to build directed networks A^q_{ij}, in which the edges also define directions (Sec. III B). Then we identified sources and sinks of extreme rainfall with a centrality measure termed network divergence Δk_i, which is the difference between the number of incoming and outgoing edges that a node has (Sec. III C). In theory, low and high values of Δk_i locate the sources and sinks of rainfall, respectively. Finally, we coupled Q_{ij} with the radial ranks R^r_{ij} to estimate the trajectories of the network flux (Sec. III D).

A. Event synchronization

In event synchronization of TRMM data, each spatial rainfall grid cell represents a network node. Event synchronization determines the correlation between extreme rainfall events at two grid cells i and j, as well as the time delay between them. For example, an extreme event l occurring at grid point i at time t^i_l is considered synchronized with another event m occurring at grid cell j at time t^j_m, within interval T^{ij}_{lm}. This time interval T^{ij}_{lm} is based on the shortest interval between two successive extreme events $l \pm 1$ and $m \pm 1$ in each time series:[48]

$$T^{ij}_{lm} = \frac{\min\{t^i_{l+1} - t^i_l, t^i_l - t^i_{l-1}, t^j_{m+1} - t^j_m, t^j_m - t^j_{m-1}\}}{2}. \quad (1)$$

Thus, T^{ij}_{lm} indicates the potential for linked events in the two time series, as it depends on the frequency of extreme events. Each paired link is weighted with a coefficient J_{ij} reflecting whether an event occurred first at location i ($J_{ij} = 1$) or j ($J_{\mathrm{ji}} = 0$); if they occur simultaneously at both locations, $J_{ij} = J_{\mathrm{ji}} = 0.5$. Each event is counted once through this weighting. We measure synchronization by counting the number of synchronized events in both time series $c(i|j)$ and $c(j|i)$,[48,49] which are the weighted count of the events in i and j, respectively,

$$c(i|j) = \sum_{l=1}^{s_i} \sum_{m=1}^{s_j} J_{ij}, \quad (2)$$

where s_{i} and s_{j} are the total numbers of extreme events; $c(i|j)$ and $c(j|i)$ define a strength parameter Q_{ij} between two grid cells,[48]

$$Q_{ij} = \frac{c(i|j) + c(j|i)}{\sqrt{(s_i - 2)(s_j - 2)}}, \quad (3)$$

and the delay parameter (or direction) q_{ij},

$$q_{ij} = \frac{c(i|j) - c(j|i)}{\sqrt{(s_i - 2)(s_j - 2)}}. \quad (4)$$

The strength of the event synchronization is normalized to $0 \le Q_{ij} \le 1$, whereas for the delay parameter $-1 \le q_{ij} \le 1$. For example, $q_{ij} = 1$ means that an extreme event at location i was always followed by an extreme event at grid cell j, whereas $q_{ij} = -1$ expresses this relationship in the opposite direction; q_{ij} infers the migration of extreme precipitation in the sense of directed propagation in networks.

B. Undirected and directed adjacency matrices

Strength parameter Q_{ij} expresses a correlation between two grid points. We set an arbitrary chosen threshold θ^Q_{ij} to determine the highest synchronization between two grid cells. We chose this threshold such that only 5% of the strongest correlations build the network following the examples of Malik *et al.*[43] and Stolbova *et al.*[48] From this network we derive an adjacency matrix,

$$A^Q_{ij} = \begin{cases} 1 \leftarrow Q_{ij} \ge \theta^Q_{ij} \\ 0 \leftarrow else \end{cases}, \quad (5)$$

where $A_{ij}^{Q} = 1$ denotes a link (edge) between i and j, and $A_{ij}^{Q} = 0$ denotes no link. This adjacency matrix is symmetric and has zeros along its diagonal. The edges have no ranks. We also calculate a nonsymmetrical directed adjacency matrix A_{ij}^{q} to encode the movement direction of extreme rainfall from the asymmetrical q_{ij} matrix. We select the threshold θ_{ij}^{q} in the same way as we did for the threshold for the strength parameter θ_{ij}^{Q}. However, in this case the notation of A_{ij}^{q} is different, because $-1 \le q_{ij} \le 1$.

$$A_{ij}^{q} = \begin{cases} \left.\begin{matrix} 1 \leftarrow q_{ij} \\ 0 \leftarrow q_{ji} \end{matrix}\right\} & q_{ij} \ge \theta_{ij}^{q} \\ \left.\begin{matrix} 0 \leftarrow q_{ij} \\ 1 \leftarrow q_{ji} \end{matrix}\right\} & q_{ij} \le -\theta_{ij}^{q} \\ 0 \leftarrow else & \end{cases} \tag{6}$$

C. Network flux of the directed network

In a directed network, all the edges have a direction into (k^{in}) or out (k^{out}) from a node. The asymmetry of A_{ij}^{q} allows us to compute the network divergence.[34,43]

$$\Delta k_i = k_i^{in} - k_i^{out}. \tag{7}$$

The network divergence is a centrality measure describing the difference of in-degree (the number of incoming edges of a node) and out-degree centrality (the number of outgoing edges of a node). Centrality measures are biased by spatial embedding due to distance-based costs of the edges, e.g., border cut edges that in reality exist with the outside of the study site. Centrality measures are thus distorted, unless the entire globe (without study site borders) is considered with equidistant grid; thus, we need to correct for boundary effects, e.g., using surrogate ensembles.[50] We approximated the edge-length distribution in our network A_{ij}^{q} using azimuthal distances (as integer) between nodes. We calculated the probability of an edge for each approximated distance in our network. We then generated 1000 spatially embedded random networks based on this distribution and computed the network divergence for each to estimate boundary effects[51] and used these to normalize the boundary effects.

D. Radial ranks

The R_{ij}^{r} metric is inspired by the fast marching method[52] and finds the most plausible flux direction in the spatially embedded correlation matrix of Q_{ij}. The fast marching method systematically computes the propagation times of waves from a source node in a grid.[53] It is originated from the Dijkstra's algorithm.[54] Dijkstra's algorithm computes the shortest path on a network, in which each path is assigned a cost to travel. It selects a starting node (i) with "0" travel cost and checks the cost of travelling to the neighboring nodes (j), eventually shifting the selected node (i) to the lowest cost distant neighbor ($j_{cheapest}$). The process is repeated iteratively until the final destination is reached. It is inconvenient when a continuous meshed domain is considered, since it follows a stair step pattern throughout the representative nodes of the meshed domain. The fast marching method instead runs by setting the investigation area to an arbitrary zone around the center. Retaining the Dijkstra's principle of a single-pass allowance, the fast marching method approximates the gradient between nodes, which makes it more suitable for meshed grids. Then, the selected zone of interest propagates in the marching direction stepwise with the propagation time following the cheapest path.[53] The method to determine the directions of propagation is repeated iteratively from a center point in all directions until the end point(s) is(are) reached.

We are inspired by this algorithm to determine the cost of travel in all possible directions for all the nodes in their neighborhoods. When the information flow is slow, the adaptive time interval T_{lm}^{ij} [Eq. (1)] between the two events will increase, decreasing the strength parameter Q_{ij}. High Q_{ij} means that the information transfer between the nodes is rather fast. Thus, Q_{ij} is inversely linked to the distant costs in the Dijkstra's example. A node has several potential directions, along which synchronization is high. The radial rank method approximates the gradient between an arbitrary number of nodes z_i^{inv} around the source node. We determined the cost of travel in 1°-steps of azimuthal direction for different search radii. Summing Q_{ij} radially along vectors within z_i^{inv} (in our case seven grid cells), we calculated R_{ij}^{r} for the azimuthal directions (Fig. 3). We used the intersection of the vector with a given grid cell as a weight w_{ij}^{inv} for R_{ij}^{r}:

$$R_{ij}^{r}(\varphi) = \sum_{1}^{z_i^{inv}} Q_{i'j'} \cdot w_{i'j'}^{inv} \rightarrow \ (i'j') = f(i,j,\varphi,z_i^{inv}). \tag{8}$$

We choose the vector with the maximum rank φ_i^{max} as the representative direction for the grid cell in question (Fig. 3):

$$\varphi_i^{max} = \underset{\varphi}{\text{argmax}}[R_{ij}^{r}(\varphi)]. \tag{9}$$

The network flux reveals details of Δk_i, whereas φ_i^{max} shows the paths of extreme rainfall, thus reflecting directions of synoptic weather patterns.

IV. RESULTS

In this section, we present how network measures together with our proposed radial rank metric can show extreme precipitation flux over the Japanese archipelago, and then we will discuss these results in the following discussion section.

A. Network divergence

We find that network divergence Δk_i has a northwest trend in JJ and ASON, clearly spatially separating sources and sinks of extreme rainfall in the nearly two decades that we analyzed [Figs. 4(a) and 4(b)]. The dominant motion of extreme rainfall is from southwest to northeast, roughly along the axis of the island arc and the overall gradient in mean annual rainfall. Along the source-sink transition (the dark blue line) the noise is somewhat higher in JJ than in ASON, with a distinct shift of the sink towards Kyushu [Figs. 4(a) and 4(b)]. In ASON, the sources are pushed further to the northwest compared to conditions in JJ [Fig. 4(c)]. The sinks over southern Honshu and Kyushu vanish during ASON, while

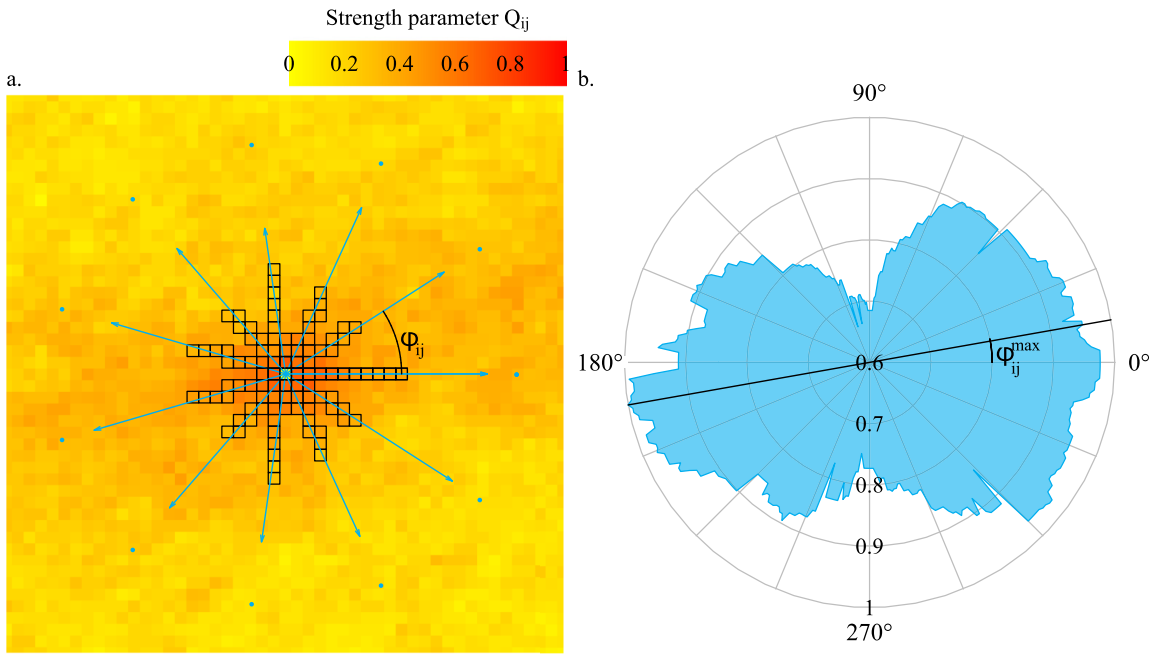

FIG. 3. (a) Sample view of an extreme rainfall grid with 11 sample vectors (we computed 360 vectors in total at 1°-intervals). The lengths of the vectors are scaled to strength parameters Q_{ij} of the first ten grid cells that the vector intersects with ($z_i^{inv} = 10$). Each grid cell has a weight w_{ij}^{inv} in this scaling, based on the intersection of the vector with that grid cell. (b) 2π domain of the radial ranks R_{ij}^r. Black line is the maximum ranked vector φ_i^{max}, which is either 11° or 191° in this example.

the source-sink transition rotates slightly clockwise centered roughly about the Japanese Alps.

B. Radial ranks

Typhoons can travel 400 to 500 km within a day. Hence, we examined R_{ij}^r over larger distances to account for effects of individual storms, guided by the size of Typhoon "Tip," which was some 2000 km in diameter and the largest recorded.[55] By default R_{ij}^r linearizes the trajectories of rainfall extremes over longer distances but remains noisy for shorter distances ($z_i^{inv} < 6$). Selecting a search radius $z_i^{inv} > 15$, however, fully masks the meandering movement of extremes. The angular deviation of φ_i^{max} is up to 45° [Figs. 4(e) and 4(f)]. Beyond a distance of about seven grid cells, φ_i^{max} converges to an azimuth within a range of 2°. We note that all angles refer to two possible directions (e.g., $3\pi/4 = -\pi/4$), since the angle is computed in $[-\pi/2, \pi/2]$.

We find that in the Sea of Japan and far eastern Asia, the general northeast flux is suppressed during JJ [Fig. 4(c)]. Directions vary between −15° and 30° but remain between 15° and 30° in the East China Sea and north of the Philippine Sea. This easterly influence decays over longer distances ($z_i^{inv} > 10$). The extreme rainfall tracks tend to follow the coastline of Honshu during both periods. In JJ, deviations increase over the Asian mainland and the Japan Sea. High deviations also occur near the 25°N parallel in JJ. In ASON, these tracks are oriented 30° ± 10° and less spread out than in JJ [Fig. 4(d)]. Local deviations from this field are north of the Philippine Sea, around southwest of Kyushu [Fig. 4(f), i], over the Japanese Alps [Fig. 4(f), ii], and at about 40°N 143°E [Fig. 4(f), iii].

V. DISCUSSION

Typhoons mainly originate in the central western Pacific and move first towards the Philippines or Taiwan before veering north to Japan, and travelling to the east once more in mature stages. Most typhoons traverse Japan from southwest to northeast,[56] influencing how extreme rainfall propagates, particularly during ASON [Fig. 5(b)]. Ninomiya[7] and Sampe and Xie[6] argued that early summer (JJ) extreme rainfall is mainly derived from east-northeast moisture transport during the Baiu Front.

The influence of the ETT is apparent in the high local deviations [Fig. 4(f), i and iii], where ETTs form two groups within ±1.5° of azimuthal direction (n > 50). About a third of all the ETTs move northwest [southeast in Fig. 4(d); circular mean $\mu_{c1} = -47^\circ \pm 30^\circ$, the error margin is the circular standard deviation], while the others move northeast ($\mu_{c2} = 56^\circ \pm 21^\circ$) around southwest of Kyushu [Fig. 4(f), i]. Although nearly all the ETTs point to the northeast in Fig. 4(f), iii, they form two equally probable clusters ($\mu_{c1} = 73^\circ \pm 11^\circ$ and $\mu_{c2} = 31^\circ \pm 10^\circ$). The spread is higher between 24° and 30°N in both periods and reflects at least two distinct groups of ETT [$\mu_{c1} = -39^\circ \pm 32^\circ$, $\mu_{c2} = 54^\circ \pm 27^\circ$; Figs. 4(e) and 4(f)], although ETTs tend to converge north of >30°N. The high angular deviation over the Japanese Alps [Fig. 4(f), ii] might reflect orographic effects on rainfall.[49]

Underlying factors that generate rainfall within a typhoon vary, due to cyclonic wind speed, vertical wind shear, and land–sea contrast (surface friction, moisture supply). These factors are closely linked to the angular deviation of maximum radial ranks φ_i^{max}. When there is a large-scale vertical wind shear (e.g., in mid-latitudes, westerlies), a convection

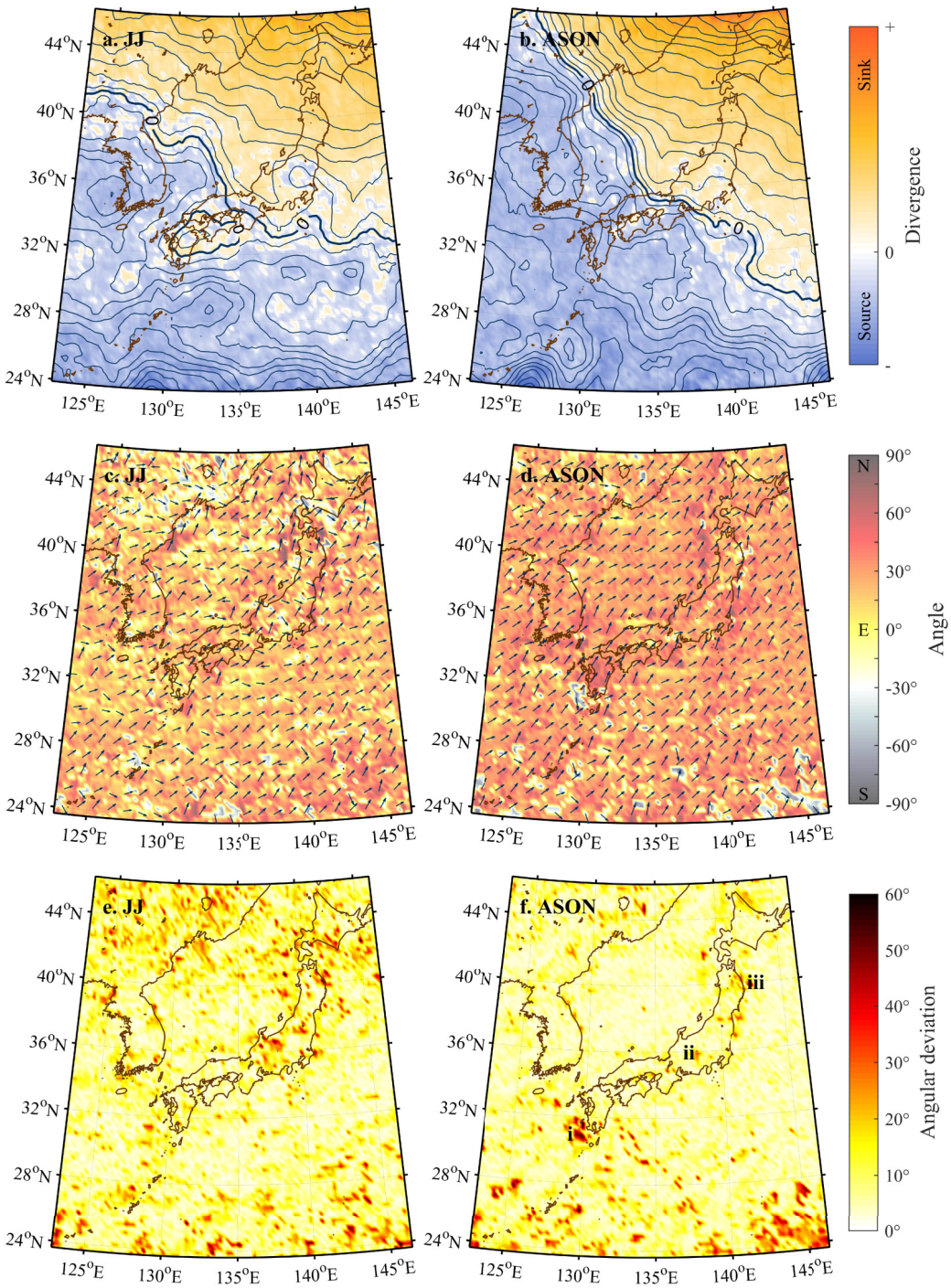

FIG. 4. [(a) and (b)] Network divergence Δk_i in JJ (a) and ASON (b), defined as the difference of incoming and outgoing links at each grid cell. Positive (negative) values are sinks (sources) in the directed network. Contours are irregularly spaced for visual aid. [(c) and (d)] Maximum radial ranks φ_i^{max} based on seven grid cells ($z_i^{inv} = 7$) for JJ (c) and ASON (d). Tones of orange are φ_i^{max} directions from southwest to northeast (or opposite); tones of gray are φ_i^{max} directions from southeast to northwest (or opposite). [(e) and (f)] Angular deviation of φ_i^{max} for step-wise extension of radial ranks from 7 ($z_i^{inv} = 7$) to 15 grid cells ($z_i^{inv} = 15$) (nine angles for each grid cell); σ_c is the circular standard deviation of all directions for JJ (e) and ASON (f). Divergent zones with high angular deviation are marked as "i," "ii," and "iii."

maximum is expected on the right hand side of the shear vector,[19,57] while a decrease in the velocity might enhance the rainfall intensity.[58] In the western North Pacific, most intense rains were observed on the right side of the eye due to the frictional convergence at the coastal terrains; wind retardation on the onshore side (creating surface convergence) and wind acceleration (creating surface divergence) on the offshore side.[59]

Westerly frontal storms influence the maximum radial ranks φ_i^{max} during JJ, despite some five typhoons per year on average that add to the variability of φ_i^{max} [Fig. 4(c)]. This variability is higher on the Sea of Japan, where we expect

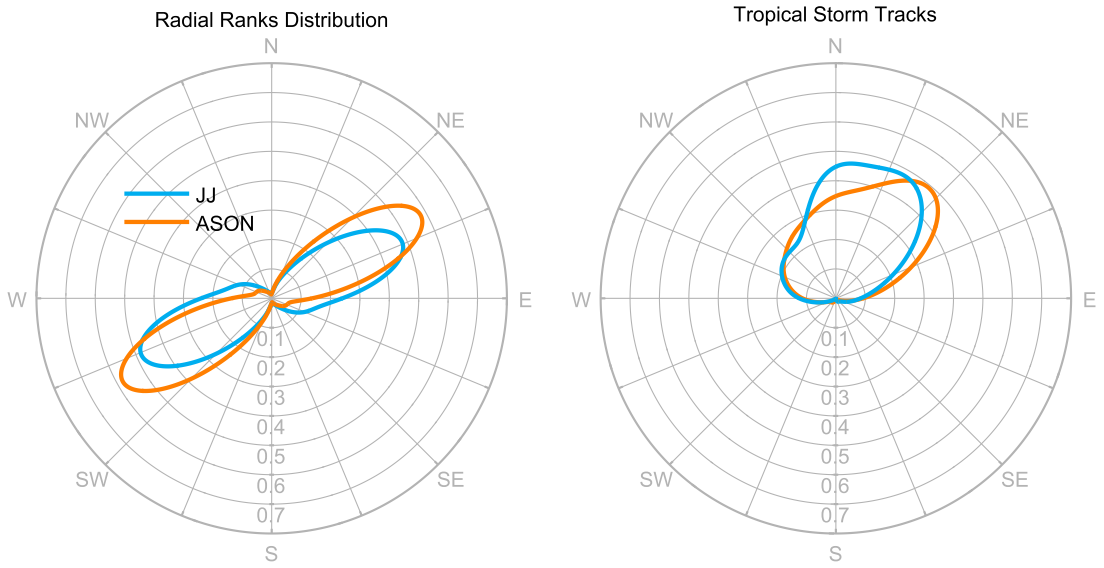

FIG. 5. Azimuthal directions of maximum radial ranks φ_i^{max} of extreme rainfall (left) compared to those of eye-of-the-typhoon tracks (ETTs, right). Probability density functions are estimated from kernel densities.

high σ_c given the influence of westerly frontal storms. Values of φ_i^{max} tend to reflect the coastline configuration of the Japanese islands [Figs. 4(c) and 4(d)]. However, ETTs influence the propagation of rainfall extremes as far as northern Honshu and seem to push rainfall extremes further east. This influence increases for higher search radii z_i^{inv} [Fig. 4(f), iii].

Overall, our method objectively highlights an angular deviation of $\sim 10°$ of radial-rank-derived extreme rainfall tracks from ETT (Fig. 5, ASON), supporting Shimazu's[22] notion of a northeast to southeast deviation of the inner rain shield. Similarly, Houze[60] noted that the most of the inner rain shields of Hurricanes "Katrina" and "Rita" were also located around east of the eye.[61] Clearly, the extreme rainfall does not systematically follow the ETT (Fig. 5, ASON) but occurs mainly east-northeast of the eye. In JJ, however, the rainfall extremes are more widely spread, possibly compromising their automatic tracking during that season.

The source-sink relation also reveals a moisture source in the northern Philippine Sea [Figs. 4(a) and 4(b)] in both periods (ASON, JJ), which we interpret as linked to the Asian monsoon. Frontal rainfalls instead come from the East China Sea, though ETTs follow a similar direction. In ASON, this source area extends northeast [Fig. 4(b)], possibly showing a more poleward monsoonal influence.[4] Northern Japan receives more than half of its rain during ASON [Fig. 1(b)], which explains the strong sink in [Fig. 4(b)]. Although this rainfall contribution in the high latitudes is mostly delivered by recurving typhoons over the western North Pacific, the influence of the westerlies on higher latitudes may further generate heavy rainfall while the typhoons lose energy. The sharper transition between the source and sink in ASON (as opposed to JJ) may reflect the role of typhoons over the study area, since the flux is based on a single moisture body. Smaller frontal storms, in contrast, would produce more scatter in the data as in JJ [Fig. 4(c)]; these storms can form rapidly depending on the presence of moisture linked to, for example, jet streams[62] or atmospheric modes.[63] In turn, adjacency matrix A_{ij}^q may contain edges regardless of moisture transfer along them.

Kyushu receives the heaviest rains during JJ [Fig. 1(c)], which explains the local sink zone in Fig. 4(a). Sinks around Kyushu in JJ change into sources in the transition to ASON [Fig. 4(b)], partly showing the northward shift of the Baiu front.[64] This is related to the shifting of the subtropical jet in late July,[65] and to increasingly active typhoons that push the sink zones northeast compared to the pattern in JJ. Although the influence of typhoons is apparent in Δk_i [Fig. 4(a)], future work needs to map the effects of individual ETT on extreme rainfall tracks. Nonetheless, we find that directed networks objectively identify regional patterns of extreme rainfall in frontal storms and typhoons and allow masking out contributions of local convective storms that hardly change their position.

VI. CONCLUSIONS

We used complex networks to track extreme rainfall propagation over Japan and its surrounding seas. Directed networks reveal regional sources and sinks of extreme weather patterns. Moreover, we introduced radial ranks R_{ij}^r to extend this approach, and to determine the details of the direction of rainfall extremes linked to typhoons [Fig. 4(d)]. R_{ij}^r is easy to set up and can mimic the network flux on large spatial scales. It requires prior knowledge about the dominant atmospheric patterns to confidently select the final direction of the flux. Derived rainfall tracks mimic the dominant southwest-northeast trend of typhoons and also Japan's mean rainfall gradient in ASON. This pattern is noisier when the more westerly frontal storms are active in JJ. Our network analysis captured an angular deviation of rainfall tracks from ETT (Fig. 5), supporting the observations of Shimazu.[22] Consequently, the lower spread of maximum radial ranks φ_i^{max} may aid tracking extreme rainfall during the typhoon season.

ACKNOWLEDGMENTS

We thank Irene Crisologo, Aljoscha Rheinwalt, and Bedartha Goswami for helping with some of the computations. Our research is funded by the Deutsche Forschungsgemeinschaft (DFG) within the Research Training Group "Natural Hazards and Risks in a Changing World (NatRiskChange)" (DFG GRK 2043/1) at the University of Potsdam.

[1]S. Kanae, T. Oki, and A. Kashida, J. Meteorol. Soc. Jpn. **82**, 241 (2004).
[2]H. Saito, O. Korup, T. Uchida, S. Hayashi, and T. Oguchi, Geology **42**, 999 (2014).
[3]E. Fukui, Geogr. Rev. Jpn. **43**, 581 (1970).
[4]R. Krishnan and M. Sugi, J. Meteorol. Soc. Jpn. **79**, 851 (2001).
[5]J. Matsumoto, Int. J. Climatol. **9**, 407 (1989).
[6]T. Sampe and S.-P. Xie, J. Clim. **23**, 113 (2010).
[7]R. Ninomiya, J. Meteorol. Soc. Jpn. **62**, 880 (1984).
[8]T. Nakazawa, SOLA **2**, 136 (2006).
[9]M. Heistermann, I. Crisologo, C. C. Abon, B. A. Racoma, S. Jacobi, N. T. Servando, C. P. C. David, and A. Bronstert, Nat. Hazards Earth Syst. Sci. **13**, 653 (2013).
[10]P. J. Webster, Science **309**, 1844 (2005).
[11]J.-H. Kim, C.-H. Ho, M.-H. Lee, J.-H. Jeong, and D. Chen, Geophys. Res. Lett. **33**, L18706 (2006).
[12]H. Murakami, B. Wang, and A. Kitoh, J. Clim. **24**, 1154 (2011).
[13]A. Manda, H. Nakamura, N. Asano, S. Iizuka, T. Miyama, Q. Moteki, M. K. Yoshioka, K. Nishii, and T. Miyasaka, Sci. Rep. **4**, 5741 (2014).
[14]M. Grossman and M. Zaiki, Weather **64**, 315 (2009).
[15]M. J. Grossman, M. Zaiki, and S. Oettle, Pap. Appl. Geogr. **2**, 352 (2016).
[16]T. R. Knutson, J. L. McBride, J. Chan, K. Emanuel, G. Holland, C. Landsea, I. Held, J. P. Kossin, A. K. Srivastava, and M. Sugi, Nat. Geosci. **3**, 157 (2010).
[17]H. E. Willoughby, F. D. Marks, and R. J. Feinberg, J. Atmos. Sci. **41**, 3189 (1984).
[18]T. Marchok, in *Third International Workshop of Tropical Cyclones–Landfall Processes, 8.1: Summary of Recent Research Related to Rainfall*, (NOAA/GFDL, Princeton, NJ, 2014); available at https://www.wmo.int/pages/prog/arep/wwrp/new/documents/RR_T8.1.pdf
[19]Y. Li, K. K. W. Cheung, and J. C. L. Chan, Q. J. R. Meteorol. Soc. **141**, 396 (2015).
[20]D. A. Hence and R. A. Houze, J. Atmos. Sci. **69**, 2644 (2012).
[21]Z. Yu, Y. Wang, and H. Xu, J. Appl. Meteorol. Climatol. **54**, 117 (2015).
[22]Y. Shimazu, J. Meteorol. Soc. Jpn. Ser II **76**, 437 (1998).
[23]J. D. Phillips, W. Schwanghart, and T. Heckmann, Earth-Sci. Rev. **143**, 147 (2015).
[24]K. Steinhaeuser and A. A. Tsonis, Clim. Dyn. **42**, 1665 (2014).
[25]N. Marwan and J. Kurths, Chaos Interdiscip. J. Nonlinear Sci. **25**, 097609 (2015).
[26]B. Sivakumar and F. M. Woldemeskel, Hydrol. Earth Syst. Sci. **18**, 4565 (2014).
[27]M. J. Halverson and S. W. Fleming, Hydrol. Earth Syst. Sci. **19**, 3301 (2015).
[28]S. K. Jha, H. Zhao, F. M. Woldemeskel, and B. Sivakumar, J. Hydrol. **527**, 13 (2015).
[29]A. Agarwal, N. Marwan, M. Rathinasamy, B. Merz, and J. Kurths, Nonlinear Process. Geophys. **24**, 599 (2017).
[30]S. Abe and N. Suzuki, Eur. Phys. J. B **59**, 93 (2007).
[31]T. Heckmann, W. Schwanghart, and J. D. Phillips, Geomorphology **243**, 130 (2015).
[32]J. F. Donges, H. C. H. Schultz, N. Marwan, Y. Zou, and J. Kurths, Eur. Phys. J. B **84**, 635 (2011).
[33]A. A. Tsonis and K. L. Swanson, Nonlinear Process. Geophys. **19**, 559 (2012).
[34]N. Boers, B. Bookhagen, H. M. J. Barbosa, N. Marwan, J. Kurths, and J. A. Marengo, Nat. Commun. **5**, 5199 (2014).
[35]A. A. Tsonis and P. J. Roebber, Phys. Stat. Mech. Appl. **333**, 497 (2004).
[36]J.-P. Onnela, A. Chakraborti, K. Kaski, J. Kertész, and A. Kanto, Phys. Rev. E **68**, 056110 (2003).
[37]J.-P. Onnela, K. Kaski, and J. Kertész, Eur. Phys. J. B Condens. Matter **38**, 353 (2004).
[38]A. A. Tsonis, K. L. Swanson, and P. J. Roebber, Bull. Am. Meteorol. Soc. **87**, 585 (2006).
[39]S. M. Papalexiou, D. Koutsoyiannis, and C. Makropoulos, Hydrol. Earth Syst. Sci. **17**, 851 (2013).
[40]*Nonlinear Time Series Analysis in the Geosciences: Applications in Climatology, Geodynamics and Solar-Terrestrial Physics* edited by R. V. Donner and S. M. Barbosa (Springer, Berlin, 2008).
[41]J. F. Donges, Y. Zou, N. Marwan, and J. Kurths, EPL Europhys. Lett. **87**, 48007 (2009).
[42]R. Q. Quiroga, T. Kreuz, and P. Grassberger, Phys. Rev. E **66**, (2002).
[43]N. Malik, B. Bookhagen, N. Marwan, and J. Kurths, Clim. Dyn. **39**, 971–987 (2012).
[44]N. Boers, A. Rheinwalt, B. Bookhagen, H. M. J. Barbosa, N. Marwan, J. Marengo, and J. Kurths, Geophys. Res. Lett. **41**, 7397 (2014).
[45]D. T. Bolvin and G. J. Huffman, *Transition of 3B42/3B43 Research Product from Monthly to Climatological Calibration/Adjustment* (NASA, 2015).
[46]E. Im, J. Ahn, and S. Jo, Clim. Res. **63**, 249 (2015).
[47]C. M. Castellano and A. T. DeGaetano, Int. J. Climatol. **36**, 1797 (2016).
[48]V. Stolbova, P. Martin, B. Bookhagen, N. Marwan, and J. Kurths, Nonlinear Process. Geophys. **21**, 901 (2014).
[49]N. Malik, N. Marwan, and J. Kurths, Nonlinear Process. Geophys. **17**, 371 (2010).
[50]J. Heitzig, J. F. Donges, Y. Zou, N. Marwan, and J. Kurths, Eur. Phys. J. B **85**, 38–59 (2012).
[51]A. Rheinwalt, N. Marwan, J. Kurths, P. Werner, and F.-W. Gerstengarbe, EPL Europhys. Lett. **100**, 28002 (2012).
[52]J. A. Sethian, Proc. Natl. Acad. Sci. U. S. A. **93**, 1591 (1996).
[53]J. A. Sethian and A. M. Popovici, Geophysics **64**, 516 (1999).
[54]E. W. Dijkstra, Numer. Math. **1**, 269 (1959).
[55]G. M. Dunnavan and J. W. Diercks, Mon. Weather Rev. **108**, 1915 (1980).
[56]M. J. Grossman, M. Zaiki, and R. Nagata, Int. J. Climatol. **35**, 2514 (2015).
[57]K. L. Corbosiero and J. Molinari, Mon. Weather Rev. **130**, 2110 (2002).
[58]J. V. Revadekar, H. Varikoden, B. Preethi, and M. Mujumdar, Nat. Hazards **81**, 1611 (2016).
[59]S. Gao, Z. Meng, F. Zhang, and L. F. Bosart, Mon. Weather Rev. **137**, 1881 (2009).
[60]R. A. Houze, Mon. Weather Rev. **138**, 293 (2010).
[61]D. A. Hence and R. A. Houze, J. Geophys. Res. **113**, D15108 (2008).
[62]N. Kurita, T. Nakatsuka, K. Ohnishi, T. Mitsutani, and T. Kumagai, J. Geophys. Res. Atmos. **121**, 12089 (2016).
[63]S. A. McAfee and J. L. Russell, Geophys. Res. Lett. **35**, L17701 (2008).
[64]N. Sato and M. Takahashi, "Interdecadal variations of the Baiu front and summer weather in Japan," in Proceedings of the International Conference on Climate Change and Variability (Center for Climate System Research, University of Tokyo, Tokyo, Japan, 2000) pp. 171–176; available at http://kishou.u-gakugei.ac.jp/~snaoki/papers/2000/CCV/doc.html.
[65]H. Ueda, T. Yasunari, and R. Kawamura, J. Meteorol. Soc. Jpn. **73**, 795 (1995).